PERGAMON

Solid State Communications 115 (2000) 269–274

solid state communications

www.elsevier.com/locate/ssc

Molecular-scale metal wires

D. Natelson*, R.L. Willett, K.W. West, L.N. Pfeiffer

Bell Laboratories, Lucent Technologies, Murray Hill, NJ 07974, USA

Received 16 December 1999; accepted 17 March 2000 by A. Pinczuk

Abstract

We introduce a novel technique employing material deposition into nanometer-scale stencils for the fabrication of continuous wires with precisely controlled widths below 10 nm. These molecular-scale metallic structures allow the examination of localization and conductance fluctuations at new length and temperature scales. This study reports measurements of continuous AuPd alloy wires with diameters as small as 3 nm and lengths greater than 1 μm. Quantum mechanical effects in the conductance of such wires are visible at temperatures as high as 80 K.

Keywords: A. Metals; A. Nanostructures; B. Nanofabrications; D. Noise; D. Quantum localization

The study of molecular-scale structures produced using standard materials is a scientific and technological imperative. While a variety of techniques exist for fabricating feature sizes below 0.1 μm (e.g. electron beam lithography (EBL) [1], scanning probe lithography [2], step edge lithography [3,4], electrodeposition into etched particle tracks [5]), forming wires microns in length with uniform widths significantly less than 20 nm has been extremely difficult. Most specialized techniques for producing molecular-scale features (e.g. atomic manipulation with a scanning tunneling microscope) result in devices that are difficult to link to larger connections for measurement purposes. Here we describe a method that uses the precision of molecular beam epitaxy (MBE) to create nanometer scale mechanical templates for material deposition, resulting in nanowires. The lateral size of these wires is limited by atomically accurate MBE layering, while wire lengths can be quite large. This combination of length and lateral definition facilitates the use of standard electrical measurement techniques, allowing critical examination of wire properties.

This study focuses on normal metal nanostructures fabricated with this method. A fundamental goal of this effort is to explore metallic structures of extremely small dimensions where quantum effects are expected to determine device properties. Quantum corrections to electrical transport properties become relevant when the electron phase coherence length, L_ϕ, becomes comparable to sample dimensions. Because L_ϕ can be much longer than the Fermi wavelength, quantum effects influence molecular-scale conductors even when the number of conducting channels, N, is still quite large ($N \sim 500$ in a normal metal wire of diameter $d = 3$ nm). Metal nanostructures with dimensions below 10 nm, potentially technologically relevant within 20 years, allow the study of disordered conductors at this previously unexplored length scale. Open questions remain concerning localization [6–8], electron–electron interactions (EEI) [9] and quantum decoherence [10] in quasi-one-dimensional systems ($d < L_T \equiv \sqrt{\hbar D/k_B T} \ll L$, where D is the electron diffusion constant and L is sample length). In particular, it is not clear that the treatment of weak localization (WL) with dephasing due to EEI, apparently successful in some semiconductor systems [11], adequately describes the behavior of traditional metals [12] as $T \to 0$ and $R(L_\phi(T)) \to h/e^2$. Conductors narrower than those made with traditional techniques will allow examination of localization at new length and temperature scales.

Further reduction of wire size also enables sensitive investigations of transport noise. Low temperature universal conductance fluctuations (UCF) due to scattering site motion [13–16], readily seen in systems with low carrier densities [17,18], should be enhanced in wires with $d < L_\phi$ since all carrier trajectories are constrained to pass within a coherence length of every active site [19]. Further, this scatterer motion may be intimately tied to the problem of decoherence [20,21]. Coherence information inferred from UCF provides a consistency check for the WL measurements

* Corresponding author. Fax: +1-908-582-7660.
E-mail address: natelson@lucent.com (D. Natelson).

0038-1098/00/$ - see front matter
PII: S0038-1098(00)00136-8

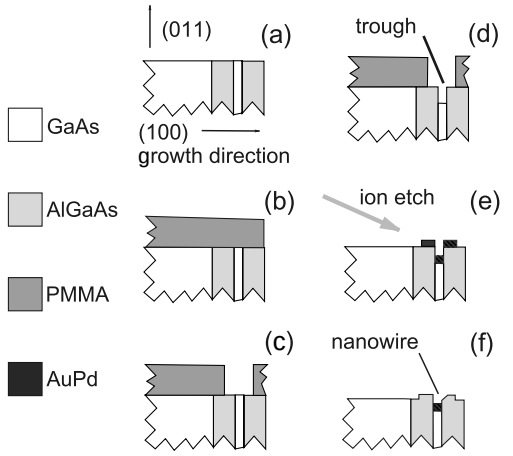

Fig. 1. A schematic representation of the wire fabrication process, showing cross-sectional views of a sample. The individual steps are described in the text.

mentioned above [22]. Nanowires approaching the molecular scale allow such testing of mesoscopic theory in this new regime.

We have produced electrically continuous AuPd wires greater than 1 μm in length with widths below 5 nm. Smaller in width than multiwalled carbon nanotubes, these wires are among the first engineered metallic structures in the molecular size regime. These structures are robust to temperature cycling and can withstand large current densities, indicative of their uniformity. We present data showing substantial quantum mechanical $R(T)$ corrections and conductance fluctuations at temperatures approaching 100 K. The field scale of the WL magnetoconductance is very large in these wires, consistent with their extremely small diameters. These results reflect the first use of a powerful method employing standard material deposition onto controlled molecular-scale surface relief.

Wire fabrication, as outlined in Fig. 1, utilizes selective etching of a prescribed layer of MBE growth to create a stencil for deposition. We start with an undoped GaAs (100) substrate, on which is grown a simple structure, in this case 2 μm of $Al_{0.3}Ga_{0.7}As$, a GaAs layer of thickness d, and an additional 2 μm of AlGaAs. We cleave strips and work on the (011) surface. Fig. 1a shows a close-up view of the cross-section of such a cleaved wafer.

Through an EBL-defined window in a polymer resist, a wet etch[1] is applied which selectively attacks GaAs, creating a trough as shown in Fig. 1d. Trough width is d, fixed by the MBE growth, while trough depth is set by the duration of the wet etch. TEM examinations reveal that the troughs' sidewalls are vertical and smooth, and the trough interior width agrees with the nominal value to better than 5%. A trough depth to width ratio between 2 and 3 is used.

Metal that will form the wire is then deposited onto the etched (011) surface using e-gun evaporation at normal incidence with no substrate cooling. Successful deposition is also achieved with magnetron sputtering, which expands the variety of accessible wire materials. The wires discussed below were made from evaporated $Au_{0.6}Pd_{0.4}$ alloy (AuPd), a well-studied material [23] known to have a grain size below 5 nm. Similar wires have also been made from both evaporated and sputtered Pt.

After liftoff the sample is placed in a reactive ion etcher (RIE) at an angle and exposed to an unneutralized N_2 plasma with a large dc bias (300–500 V), which functions as a highly directional etch; see Fig. 1e. Sample orientation is such that the bottom of the trough is protected from the etch, while the metal outside the trough is sputtered away. At the end of this process, Fig. 1f, there is a metal wire remaining in a trough on the (011) surface. To measure device electrical properties, a lead frame is defined on the cleaved surface using EBL and formed by evaporation of 2.5 nm Ti and 90 nm Au followed by liftoff.

A scanning electron microscope (SEM) image of a 20 nm diameter AuPd wire and lead structure is shown in Fig. 2; some of the surrounding template material has been removed to allow direct viewing of the wires, using a wet etch[2] which attacks both GaAs and AlGaAs but does not react with the wires or leads. The mottled rectangular region is the EBL-defined area onto which the AuPd was evaporated. In the measurements discussed below, no overall wet etch was employed, leaving the wires undisturbed in the troughs used for their fabrication.

Comparison of two- and four-terminal results shows that the contact resistances between the leads and the wires are usually less than 10 Ω. The wire resistances are always *higher* than predictions using nominal wire dimensions and resistivities, understandable since any inhomogeneity is expected to reduce the wire cross-section from its ideal value. The wires are robust, often withstanding dc current densities approaching 10^{13} A/m^2 before failing. SEM examination of wires after such failures was fruitful, indicating unequivocally that the current passes through the wire and not some unintended shunt.

Using this technique, we have successfully fabricated a variety of samples from AuPd and Pt on which we have performed 4-terminal measurements. Widths included 5, 7.5, 10, 12.5, 15, 20, and 30 nm, with lengths ranging from 0.5 to several μm. The data which follow come from a particular codeposited wire set; we used the edge technique to make wires of widths 5 and 20 nm, and standard EBL for larger widths. These samples and a control 2D film were deposited in a single AuPd evaporation of 7.5 nm thickness

[1] 500 ml 30% H_2O_2, 400 μl 30% NH_4OH, which etches bulk GaAs at approximately 50 nm/min.

[2] 100 ml distilled H_2O, 10 ml 30% H_3PO_4, 2 ml 30% H_2O_2, which etches GaAs and AlGaAs at approximately 100 nm/min.

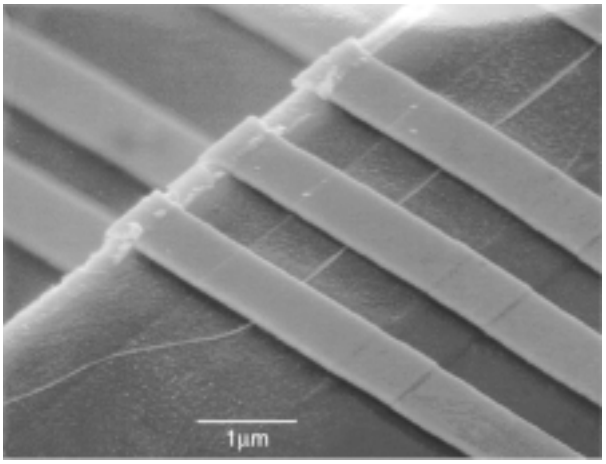

Fig. 2. An SEM micrograph of a 20 nm wide AuPd wire spanning several 0.5 μm-wide Au leads, after a wet etch to remove surrounding wafer material. The wire segment at the bottom of the photo is not attached to a second lead and is free of the substrate.

on top of a 1 nm Ti adhesion layer. Low temperature measurements of the wires employed a 4-terminal ("Kelvin") bridge technique with a lock-in amplifier as a phase-sensitive detector. Continuous wires 3 nm wide have been fabricated by deposition of 5 nm of AuPd but have only been examined with two-terminal measurements and are therefore excluded from the ensemble presented below.

We begin by considering measurements of R vs. T and move on to resistance noise ($R(t)$) and magnetoresistance behavior, discussing the data in the context of current mesoscopic theory. As will become clear, the smallest samples made with this technique demonstrate relatively large quantum mechanical effects in their conductance at temperatures as high as 80 K.

Measurements of the low temperature resistivity of the coevaporated film ($\rho \approx 25.1\ \mu\Omega$ cm were combined with free-electron model parameters for pure Au [24] using the Einstein relation to estimate roughly D and l. Note that this value of ρ is consistent with (and lower than) the values reported by previous researchers [23] for similar material deposited by evaporation. Assuming that AuPd alloy has an electronic density of 5.9×10^{28} m^{-3} and a Fermi velocity of 1.5×10^6 m/s, we find $D = 1.5 \times 10^{-3}$ m^2/s and $l \approx 3$ nm. This estimate of l, while short, is unsurprising considering the grain size and substitutional disorder of the AuPd alloy. Boundary scattering may be relevant in wires approaching this scale. Using this value of D to compute L_T, we find that the 5 nm wire should satisfy $L_T > d$ even at room temperature.

Fig. 3 shows the fractional change in resistance from 300 K as a function of temperature for samples of various dimensions with no applied magnetic field. The 300 K resistances per unit length of the various samples are indicated in the caption. Two features are of particular interest: first is the overall temperature dependence of the resistance, including a rise in R at low temperatures for the 5 and 20 nm width samples (below 80 and 12 K, respectively). The overall change in R with T is depressed as wire size decreases, consistent with boundary scattering affecting the elastic mean free path in the smallest wires. The low temperature resistance rise is considerably more pronounced and occurs at higher temperatures for wires of smaller cross-section. The second notable effect is the increase in measured resistance noise as T is lowered, again more

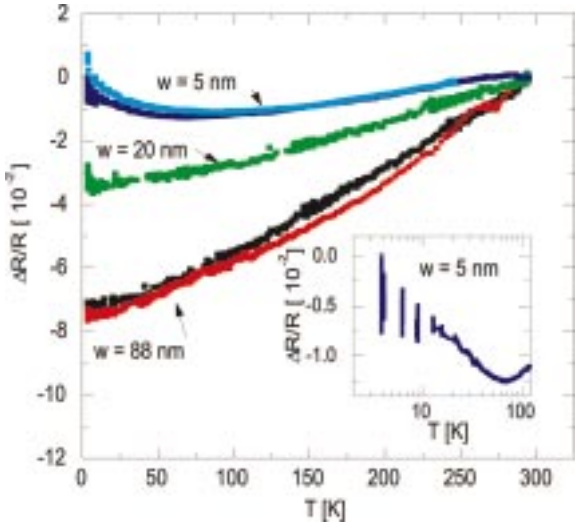

Fig. 3. Fractional change in resistance as a function of temperature, for wires consisting of 7.5 nm of AuPd, with various widths as indicated. Resistances at 300 K: $R(w = 5\text{ nm}, L = 0.75\ \mu\text{m}) = 10243\ \Omega$; $R(w = 5\text{ nm}, L = 1.5\ \mu\text{m}) = 19200\ \Omega$; $R(w = 20\text{ nm}, L = 0.75\ \mu\text{m}) = 2353\ \Omega$; $R(w = 88\text{ nm}, L = 0.75\mu\text{m}) = 387.4\ \Omega$; $R(w = 88\text{ nm}, L = 1.5\ \mu\text{m}) = 791\ \Omega$. The inset replots the data for one of the 5 nm wires, using a logarithmic axis for clarity.

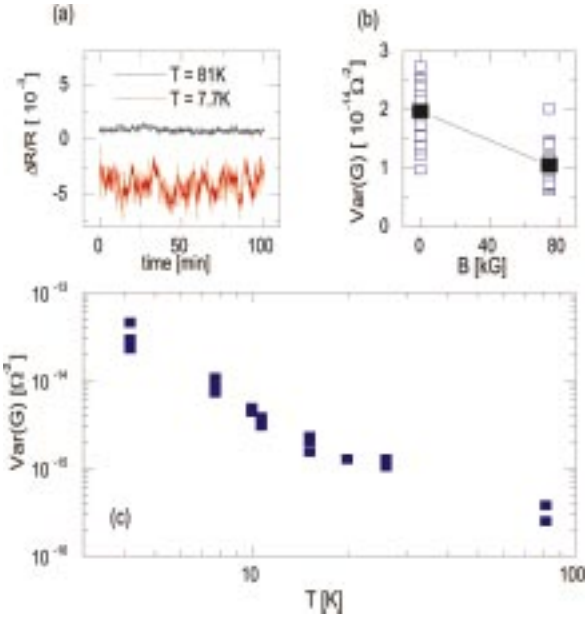

Fig. 4. Temporal noise in measured resistance of a 5 nm wide, 0.75 μm long wire. (a) Noise as a function of time for this wire segment at two different temperatures. (b) Noise as a function of applied perpendicular magnetic field at 4.2 K; black points are the average variance values. (c) Noise as a function of temperature.

severe in smaller samples. The inset is a rescaled plot of the data for one of the 5 nm wires, clearly demonstrating both the resistance rise and noise behaviors.

The pronounced low-T resistance rise is not due to Kondo behavior from magnetic impurities since such a bulk effect would be manifested in the codeposited film. Electron–electron interactions are expected to contribute to such a resistance rise as $T \rightarrow 0$ by causing a decreased density of states at the Fermi level [8]. This effect arises because the diffusive motion of the electrons enhances their interactions compared to the free plane wave case, with L_T setting the relevant length scale. The predicted form of the resistance rise is

$$\frac{\Delta R}{R_0} = \frac{1}{\sqrt{2}}(4 - 1.5F)\frac{e^2}{h}\frac{R_0}{L}L_T \sim T^{-1/2},$$

where F is a screening parameter between 0 and 1, and R_0 is the sample resistance at a reference temperature low enough that the carrier mean free path is not affected by electron–phonon scattering. The data are roughly consistent with a $T^{-1/2}$ dependence below ~25 K, though the measured resistance rise from 25 to 4.2 K is 2.5–4 times smaller than that predicted above.

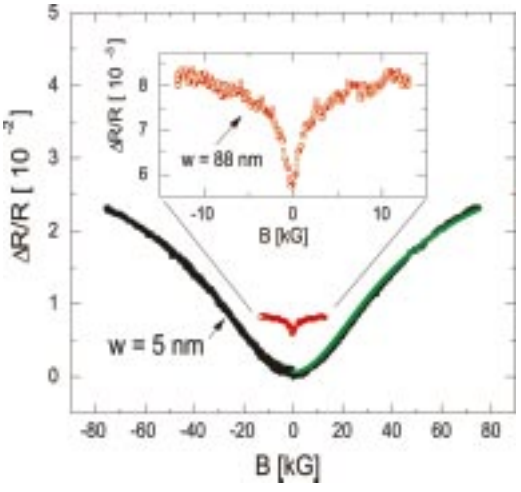

Fig. 5. Resistance as a function of perpendicular magnetic field at 4.2 K for two different wire widths, vertically offset for clarity. The green curve is a fit of the 5 nm width wire data to the theoretical expression cited in the text for one-dimensional weak localization with strong SO scattering; the fit value of the Nyquist time is 7.4×10^{-13} s. The inset shows a magnified view of the data for the 88 nm wide sample.

Fig. 4a shows R as a function of time for a 5 nm wide 0.75 μm long wire segment at two different temperatures. This clearly demonstrates the resistance noise shown in the inset of Fig. 3, which we interpret as UCF.

Universal conductance fluctuations exist because the conductance in the quantum case is sensitive to the phase differences between the many possible carrier trajectories. Scattering site motion can cause UCF, and that is the proposed origin of the noise behavior in question. In the limit that the entire scatterer configuration effectively changes, one expects a conductance change $(\delta G)^2 \sim (e^2/h)^2$. The measured $\langle \delta G^2 \rangle$ is expected to be reduced

from this value by ensemble averaging ($L_\phi < L$) and thermal smearing ($k_B T > \hbar D/L_\phi^2$) [25]. Decreasing T is expected to increase L_ϕ and reduce thermal smearing, leading to growing UCF. In the presence of a magnetic field large enough to thread at least one flux quantum through a typical coherence volume, $\langle \delta G^2 \rangle$ is predicted to be reduced by a further factor of 2. Time-domain UCF indicate nonclassical contributions to the conductance and allow additional checks on the physics of decoherence.

To quantify the resistance noise, we performed one resistance measurement every 3 s (limiting our bandwidth to frequencies below ~0.3 Hz), and binned the data into thousand-point sets. For each set we then computed an average conductance and a variance $\langle \delta G^2 \rangle$. Fig. 4c shows the measured $\langle \delta G^2 \rangle$ for the 5 nm wide wire segment as a function of temperature. The magnitude of this behavior is consistent with UCF and a growing L_ϕ as T is decreased. Note that the noise is detectable at temperatures in excess of 50 K. Further, in Fig. 4b we plot many 4.2 K measurements of $\langle \delta G^2 \rangle$ at both zero field and at a field of 7.5 T applied perpendicular to the length of the wire. The black points show the average variance at each field value, which does exhibit a decrease at high fields. The detection of UCF noise over this temperature range demonstrates the importance of quantum conductance effects when nanostructure size is reduced below 10 nm. In larger metal structures it is usually necessary to work at temperatures below 1 K to observe such clear resistance behavior without specialized noise measurement techniques [26].

Fig. 5 shows the 4.2 K resistance vs. applied magnetic field for a 5 nm wide wire segment and an 88 nm wide lithographically defined wire (magnified in the inset). Both the field scale and the overall size of the resistance change are roughly ten times larger in the 5 nm case. The size and form of the 5 nm data are well described in terms of one-dimensional WL, in which interference between pairs of time-reversed trajectories leads to a correction to the conductivity [9]. An applied magnetic field breaks time reversal symmetry, and the correction to the conductivity therefore has a strong field dependence: the weak localization magnetoresistance (MR). The functional form of the MR is set by the effective dimensionality of the system and the strength of spin–orbit (SO) scattering. The field scale of the WL is strongly influenced by the wire diameter d, while the overall magnitude of $\Delta R/R_0$ is dominated by the resistance per unit length and the dephasing times (which are the Nyquist time τ_N from EEI, and the contribution from all other dephasing processes, $\tau_{\phi 0}(H = 0)$) [9,27]. The MR data for the 5 nm wire are fit very well using just the Nyquist time as a fitting parameter, and assuming all other dephasing processes are slow (setting $\tau_{\phi 0}(H = 0) = 10$ ns, for example). Boundary scattering would modify the effective D used in fitting the data. The field scale of the measured magnetoresistance is a firm consistency check on the wire size, while the dephasing time and MR functional form are consistent with the WL picture in this previously unexplored size regime.

We have demonstrated a powerful, versatile, new method for producing surface relief with lateral definition at otherwise inaccessibly small widths (3 nm). Our initial investigations use such structures to produce electrically continuous deposited normal metal wires in a size regime previously restricted to molecular systems (e.g. carbon nanotubes). At the 5 nm length scale quantum corrections to electrical transport properties are detectable at temperatures as high as 80 K; additional reduction of the wire width is expected to drive these quantum effects to higher temperatures. The lower limit of width achievable with this technique is now being tested.

Beyond these efforts, the ability to fabricate long wires from a variety of metals in this size regime makes possible for the first time a large range of experiments studying phenomena at the molecular scale. The large wire length allows multiterminal device configurations, and potentially provides enough room for additional local gates or proximal deposition of other materials, such as magnetic impurities. Further, the generality of the stenciling method naturally suggests the use of other classes of materials to produce the wires instead of normal metals. Superconducting, magnetic, or other systems can be deposited through sputtering or other means, with the ultimate lower limit of wire width to be determined for each specific material.

References

[1] W. Chen, H. Ahmed, Appl. Phys. Lett. 62 (1993) 1499.
[2] M.A. McCord, R.F.W. Pease, J. Vac. Sci. Technol. B 6 (1988) 293.
[3] D.E. Prober, M.D. Feuer, N. Giordano, Appl. Phys. Lett. 37 (1980) 94.
[4] D.C. Flanders, A.E. White, J. Vac. Sci. Technol. 19 (1981) 892.
[5] W.D. Williams, N. Giordano, Rev. Sci. Instrum. 55 (1984) 410 (and references therein).
[6] D.J. Thouless, Phys. Rev. Lett. 39 (1977) 1167.
[7] D.J. Thouless, Solid State Commun. 34 (1980) 683.
[8] P. Lee, T.V. Ramakrishnan, Rev. Mod. Phys. 57 (1985) 287.
[9] B. Al'tshuler, A.G. Aronov, D.E. Khmel'nitskii, J. Phys. C 15 (1982) 7367.
[10] Y. Imry, Introduction to Mesoscopic Physics, Oxford University Press, Oxford, 1997.
[11] Yu.B. Khavin, M.E. Gershenson, A.L. Bogdanov, Phys. Rev. Lett. 81 (1998) 1066.
[12] P. Mohanty, E.M.Q. Jariwala, R. Webb, Phys. Rev. Lett. 78 (1997) 3366.
[13] S. Feng, N. Giordano, in: B.L. Al'tshuler, P.A. Lee, R.A. Webb (Eds.), Mesoscopic Phenomena in Solids, Elsevier, Amsterdam, 1991.
[14] S. Feng, P.A. Lee, A.D. Stone, Phys. Rev. Lett. 56 (1986) 1960.
[15] S. Feng, P.A. Lee, A.D. Stone, Phys. Rev. Lett. 56 (1986) 2772.
[16] S. Hershfield, Phys. Rev. B 37 (1988) 8557.

[17] D.E. Beutler, T.L. Meisenheimer, N. Giordano, Phys. Rev. Lett. 58 (1987) 1240.
[18] N.O. Birge, B. Golding, W.H. Haemmerle, Phys. Rev. Lett. 62 (1989) 195.
[19] K.S. Ralls, D.C. Ralph, R.A. Buhrman, Phys. Rev. B 47 (1993) 10 509.
[20] Y. Imry, H. Fukuyama, P. Schwab, Europhys. Lett. 47 (1999) 608.
[21] A. Zawadowski, J.V. Delft, D. Ralph, Phys. Rev. Lett. 83 (1999) 2632.
[22] D. Hoadley, P. McConville, N.O. Birge, Phys. Rev. B 60 (1999) 5617 (and references therein).
[23] J.J. Lin, N. Giordano, Phys. Rev. B 35 (1987) 545 (and references therein).
[24] C. Kittel, Introduction to Solid State Physics, 7th ed., Wiley, New York, 1996.
[25] S. Feng, in: B.L. Al'tshuler, P.A. Lee, R.A. Webb (Eds.), Mesoscopic Phenomena in Solids, Elsevier, Amsterdam, 1991, p. 131.
[26] J.H. Scofield, Rev. Sci. Instrum. 58 (1987) 985.
[27] P.M. Echternach, M.E. Gershenson, H.M. Bozler, A.L. Bogdanov, B. Nillson, Phys. Rev. B 48 (1993) 11 516.